Polymer Journal, Vol. 39, No. 2, pp. 138–146 (2007)
©2006 The Society of Polymer Science, Japan

Miscibility and Properties of Acid-Treated Multi-Walled Carbon Nanotubes/Polyurethane Nanocomposites

Chi-Hung LEE, Jia-Yi LIU, Shen-Liang CHEN, and Yen-Zen WANG†

Department of Chemical Engineering, National Yunlin University of Science and Technology, 123 University Road, Section 3, Douliou, Yunlin 64002, Taiwan

(Received September 28, 2006; Accepted November 1, 2006; Published December 14, 2006)

ABSTRACT: Nanocomposites based on polyurethane and acid-treatment multi-walled carbon nanotubes (A-MWNTs) are prepared by solution blending. The surface of the MWNTs was modified by acid treatment to incorporated functional groups. The modified MWNTs exhibited improved dispersion in organic solvents and miscibility with the PU matrix. The derivatives of MWNTs were characterized by Fourier transform infrared (FT-IR) spectroscopy, Transmission electron microscopy (TEM) and Raman spectroscopy. The thinning and defects of the A-MWNT from the surface etching of acid treatment can be clearly seen from TEM pictures and Raman spectra, respectively. The interaction and degree of miscibility between the MWNTs and the PU matrix is examined using FT-IR, modulated differential scanning calorimeter (MDSC), TEM and atomic force microscopy (AFM). The hydrogen bonding index (HBI) measured by FT-IR was employed to show the degree of interchange hydrogen bonding. Composites films with higher A-MWNT content exhibit higher HBI and the degree of miscibility is significantly improved. The resultant composites have higher tensile strength, higher Young's modulus and lower elongation at break because of the rigid structure of A-MWNT and the increase in the number of hydrogen bonds among the composites. Incorporating A-MWNT in composites increases the mass of the residue at temperatures over 600 °C, according to thermo gravimetric analysis (TGA). An A-MWNT percentage of 20 wt %, the electric conductivity approached 6.2×10^{-2} S/cm. [doi:10.1295/polymj.PJ2006121]

KEY WORDS Polyurethane / Carbon Nanotubes / Miscibility / Hydrogen Bonded /

Carbon nanotubes (CNTs) have attracted considerable interest since their preparation in 1991 by Minima,[1] owing to their exceptional electrical, physical and mechanical properties.[2–4] These nano-structural elements can also be used as nano-fillers and nano-reinforcements to improve the mechanical, thermal and impact-resistance properties to be advanced composite materials.

Since carbon nanotubes are typically insoluble in organic solvents and severely bundled, their homogeneous dispersion in desired polymer matrix is difficult to achieve. The dissolution of CNTs in common organic solvents has been described elsewhere literature,[5,6] and depends mainly on the attachment of building blocks to the carboxylic functional groups that are formed by the oxidation of CNTs by applying caustic acid.[5–7] This method has the disadvantage of cutting the CNTs into short pieces of about 100–300 nm, making them useless for any practical purposes that are based on the aspect ratio of the filler's.[5] The blending of A-MWNT with other polymers is highly active area of research, with numerous publications in recent years, aimed at combining favorable mechanical properties. One of the major limitations of the blending is that it always generates a highly heterogeneous phase-separated morphology. Therefore, blending composites to reach molecular intermixing is extremely difficult, such mixing is required to improve significantly the physical properties of the blend. Numerous investigations have described techniques of fabrication and characterization of CNTs/polymer composites with various kinds of matrix polymers, such as polyethylene,[8] polyvinyl alcohol,[9] polypropylene,[10] poly(methyl methacrylate),[11–13] epoxy[14–16] and polystyrene,[17] polyimide,[18] Nylon[19] and polyurethane.[20,21]

Zhu *et al.*[18] reported that the addition of 5 wt % Acid-treated MWNT in a polyimide matrix by a solution blending method, resulting in a 40% increase of tensile modulus, tensile strength than that of pure polyimide. The dielectric constant reaches 60, about 17 times of the 3.5 for neat polyimide. Zhang *et al.*[19] prepared an MWNT/Nylon-6 nanocomposite by a simple melt-compounding procedure. The tensile strength and hardness of the nanocomposites increase by 115, 120, and 67%, respectively. Xu *et al.*[16] also found that 0.1 wt % MWNTs in the epoxy resins increased the elastic modulus by 20%. *In situ* polymerization of waterborne urethane monomers in the presence of 1.5 wt % A-MWNT increased electrical conductivity by eight to nine orders of magnitude higher than that of waterborne polyurethane.[20] Ma *et al.*[21] prepared MWNT/waterborne polyurethane nanocomposites by covalently and ionic bonding to

†To whom correspondence should be addressed (Tel: +886-5-5342601 exit 4617, Fax: +886-5-5312071, E-mail: wingmen@yuntech.edu.tw).

CNT surface. The mechanical property tests revealed that MWNTs significantly improve the tensile properties (increasing the tensile stress by 370% and the tensile modulus by 170.6%).

In this work, the treatments is used to acidify the nanotubes' surface to various degrees, improving their chemical compatibility with polyurethane by dispersing the MWNTs effectively in polymer matrix, yielding an excellent nanotube-reinforced nanocomposite. The degree of miscibility, the mechanical properties, the thermal stability and conductivity of the composites are discussed.

EXPERIMENTAL

Materials

The MWNTs prepared by chemical vapor deposition (CVD) method were purchased from SeedChem Company (Australia) and purified to over 95% purity. The MWNTs had an external diameter of 40–60 nm, an internal diameter of 2–6 nm, and a length of 1–10 μm. The modified MWNTs were prepared in the following steps; ultrasonicating the mixture of MWNTs in 98% sulfuric acid and 70% nitric acid (volumetric ratio 3:1) at 40 °C for 12 h and 24 h, respectively; washing A-MWNTs with distilled water, and drying in a vacuum oven at 100 °C for 24 h. Polyether glycol (PTMO1000, $M_n = 1000$) and 4,4′-methylene bis (phenylisocyanate) (MDI, 98%) were obtained form Aldrich and 1,4-butanediol (1.4BD, 99.5%, Riedel-delyaën Chemical) was purified by vacuum sublimation (70 °C, 24 h). Dimethlformamide (DMF, Mallinckrodt Chemical) was distilled over anhydrous $MgSO_4$ powder at reduced pressure and sieved using 4 Å molecular sieves before use.

Synthesis of PU

PU was synthesized by pre-polymerization using certain amounts of polyether glycol (PTMO1000), 4,4′-methylene bis (phenylisocyanate) (MDI), and 1,4-butanediol (1.4BD). The PTMO1000 behaves as the soft segment, whereas the MDI and 1.4BD act as the hard segments. The prepolymer was prepared in a reaction of excess MDI with PTMO1000 at 80 °C for 90 min in a four-necked cylindrical vessel that was equipped with a mechanical stirrer. A chain extender of 1.4BD was gradually added to the prepolymers at 80 °C for 2 h, and the mixture was allowed to continue to undergo post-polymerization. PU was finally obtained after washing with methanol and being dried completely in an oven. The molar mass and molar mass distribution of the resulting PU, were measured using a gel permeation chromatogapher (GPC, Testhigh model 500) with mono-distributed polystyrene as the standard. The number average molecular weight and molecular weight distribution expressed as polydispersity index of the PU were measured by gel permeation chromatograph and turn out to be 60098 and 1.58, respectively.

Table I. The designation of PU/MWNT composites

Designation	Composites
PU	PU = 100 (wt %)
PU/neat MWNT-1%	PU:neat MWNT = 99:1 (wt %)
PU/neat MWNT-5%	PU:neat MWNT = 95:5 (wt %)
PU/neat MWNT-10%	PU:neat MWNT = 90:10 (wt %)
PU/neat MWNT-20%	PU:neat MWNT = 80:20 (wt %)
PU/A-MWNT(12 h)-1%	PU:A-MWNT(12 h) = 99:1 (wt %)
PU/A-MWNT(12 h)-5%	PU:A-MWNT(12 h) = 95:5 (wt %)
PU/A-MWNT(12 h)-10%	PU:A-MWNT(12 h) = 90:10 (wt %)
PU/A-MWNT(12 h)-20%	PU:A-MWNT(12 h) = 80:20 (wt %)
PU/A-MWNT(24 h)-1%	PU:A-MWNT(24 h) = 99:1 (wt %)
PU/A-MWNT(24 h)-5%	PU:A-MWNT(24 h) = 95:5 (wt %)
PU/A-MWNT(24 h)-10%	PU:A-MWNT(24 h) = 90:10 (wt %)
PU/A-MWNT(24 h)-20%	PU:A-MWNT(24 h) = 80:20 (wt %)

Preparation of the PU/MWNTs Nanocomposites

Various conductive fillers (neat-MWNT, A-MWNT(12 h), A-MWNT(24 h)) were initially dissolved in DMF (30 min ultrasonic treatment) and then were mixed with PU (dissolved in a DMF). After 30 min of acoustic sonication, the solution nanocomposites was stirred vigorously at 70 °C for 24 h in a four-necked flask; after the solvent was removed by vacuum (at 70 °C), the nanocomposites were then cast onto the bottom of a 150 mm × 150 mm glass plate. Table I presents compositions of the polymer and MWNT in the nanocomposites.

Characterization and Property Measurements

An excitation argon laser with a wavenumber of 514 nm was used to obtain Raman spectra of neat MWNT and A-MWNTs with a Jasco 2100 NRS spectrophotometer (Tokyo, Japan). Molecular weights and molecular weight distributions were determined using DMF as an eluent by gel permeation chromatography (GPC) using a Waters 510 HPLC-equipped with a 410 Differential Refractometer, a UV detector and three Ultrastyragel columns (100, 500, and 103 Å) connected in series to increase the pore size at a flow rate of 0.4 mi/min. The molecular weight calibration curve was obtained using polystyrene standards. Fourier Transfer Infrared Spectroscopy (FT-IR) spectra of MWNT were obtained between 400 and 4000 cm^{-1} using a Spectrum One FT-IR by Perkin Elmer. The PU/MWNT nanocomposite sample was coated on a KBr tablet. A minimum of 32 scans was averaged using a signal resolution of 2 cm^{-1} ranged from 400 to 4000 cm^{-1}. The absorption peak due to hydrogen-bonded –C=O stretching is centred at ~1730 cm^{-1}.

The extent of carbonyl absorotion group participating in hydrogen bonding is expressed by HBI, which is as the relative absorbances of the hydrogen-bonded carbonyl peak to that of free hydrogen-bonded carbonyl peak.[22–24] mechanical measurements were made on sample of size $50 \times 10 \times 0.25\,mm^3$ using a tensile machine (mode TCF-R) made by Yashima works Ltd. at a crosshead speed of 20 mm/min. At least five samples were employed to yield final data by average. The resistance (R) of the material was measured using a four-probe measurement instrument and the conductivity (σ) was obtained from the formula $\sigma = L/(R \times A)$, where L denotes the thickness and A is the cross-section area. Each sample was pressed into a disk (diameter ~1.3 cm: thickness ~1.5 mm). At least three samples were employed to yield final data by averaging. The glass transition temperatures were determined using a DuPont Q100 Modulated differential scanning calorimeter in a nitrogen atmosphere at a heating rate of 3 °C/min with a modulation of ±0.6 °C amplitude and a period of 60 s. The thermogravimetric analysis (TGA) of the samples was carried out using a DuPont Q500 TGA instrument. The analysis was performed at a heating rate of 10 °C/min in an atmosphere of nitrogen. Samples for the transmission electron microscopy (TEM) were micro-tomed using a Leica Ultracut Uct into slices with a thickness of 90 nm. Then, a carbon layer with a thickness of about 3 nm was deposited onto these slices and placed on copper nets for TEM observation. The TEM instrument was a JEOL-2000 FX, with an accelerating voltage of 200 kV.

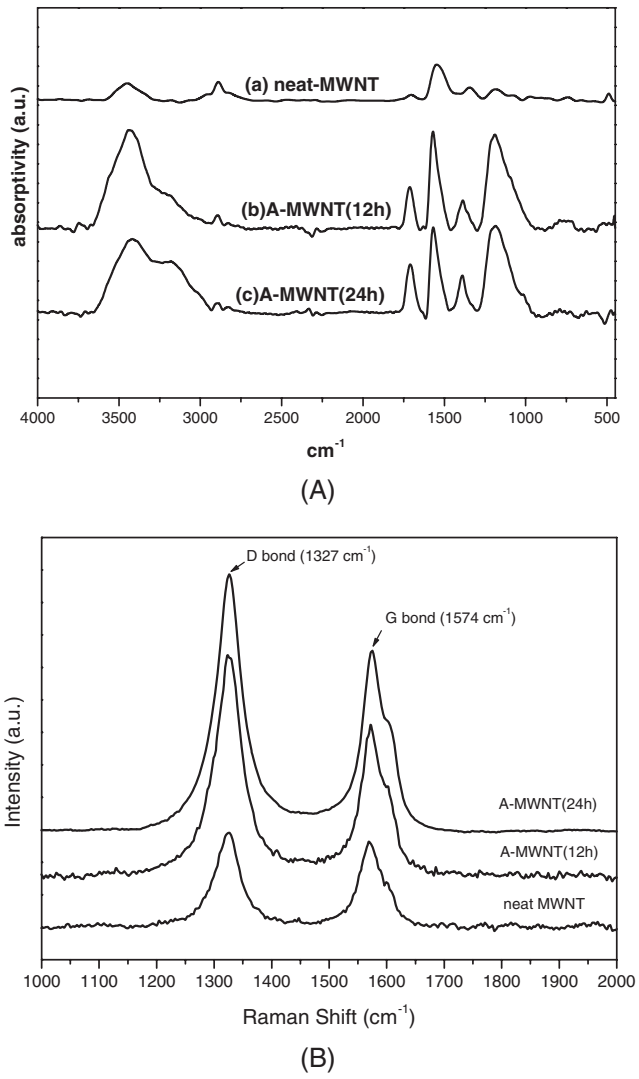

Figure 1. Characterization of functional group of the A-MWNTs of various period of acid treatment for (A) FT-IR, (B) Raman.

RESULTS AND DISCUSSION

Characterization of Acid Treated MWNT (A-MWNTs)

Curves a, b and c in Figure 1A presents the FT-IR spectra of neat and acid-treated MWNTs. The spectra of the acid-treatd MWNTs include board bands centered at 3415 cm^{-1}, corresponding to –OH stretching vibrations of C–OH groups; the bands at 1710 cm^{-1} correspond to stretching vibrations of carboxyl and carbonyl groups. A broad band centered at 1566 cm^{-1} and a shoulder at 1392–1386 cm^{-1} are assigned to deformation vibrations of O–H and C–OH groups, respectively. A weak broad band at 1210–1175 cm^{-1} is associated with C–O stretching vibrations.[25] Unlike neat MWNTs, acide-treated MWNTs are known have the carboxyl and hydroxyl groups on their surface.

Raman spectroscopy is an effective approach for characterizing the non-functionalized or functionalized CNTs. The defects created on the A-MWNT surface from acid etching can also be monitored from the changing ratio between D and G band height of their Raman spectra. As shown in Figure 1B, D- and G-bands of MWNTs at about. 1327 and 1574 cm^{-1}, attributed to the defects, the disorder-induced modes and in-plane E_{2g} zone-center mode, are clearly observed in the spectra of both neat MWNTs and acid-treatd MWNTs. Figure 1B reveals that the D-band intensity of the A-MWNTs increased with the duration time of acid treatment above that of neat MWNT. Because of the growth of disorders and defects, the D-band intensity of A-MWNT was increased with time of acid treatment. The relative height of D bond and G bond (h_D/h_G) increased with the duration of acid treatment, because of attributed to the extent of destruction of carbon nanotubes by strong acid oxidation. It also indicates that the sp^2 orbital of the planar C=C bond may be open to form a sp^3 non-planar C–C bonds, generating defects on the carbon nanotube surfaces. Figure 2 presents the TEM micrographs of neat MWNTs and A-MWNTs from 12 to 24 h. The thinning of the A-MWNT from the surface etching of acid

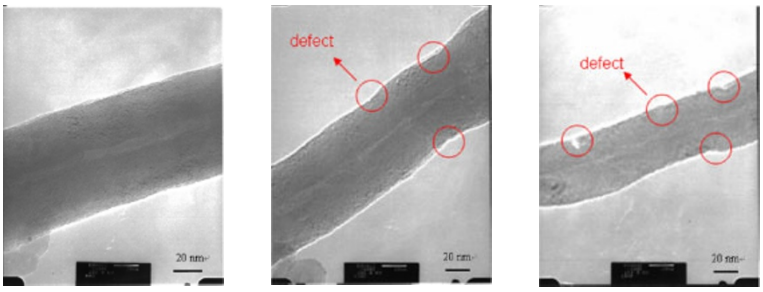

(A) (B) (C)

Figure 2. TEM micrographs of A-MWNTs with various acid-treatment duration (A) 0 h, (B) 12 h, (C) 24 h.

Table II. The external diameter of MWNT and A-MWNT as the period of acid-treatment

Designation	External diameter (nm)
Neat MWCNT	60–40
A-MWNT 12 h	40–30
A-MWNT 24 h	30–20

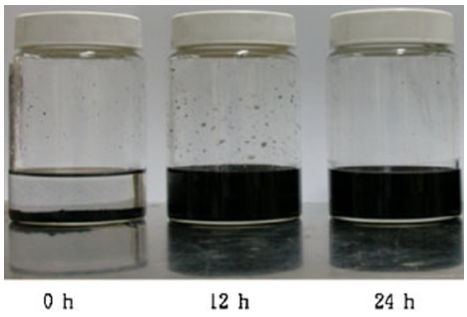

Figure 3. Photomicrograph of A-MWNTs dispersed in DMF.

treatment can be clearly seen from TEM pictures. The external diameters obtained from Figure 2 were list in Table II. The external diameters declined from 60 to 30 nm as the period of acid-treatment. Treatment created many defects since functional groups destroyed the smooth surface of neat MWNTs.

The work prepares a PU and A-MWNT-based nanocomposite with extensive quality of dispersion in the common solvents. Various MWNTs were dispersed in DMF by ultrasonic and strong magnetic stirring. Figure 3 displays the photomicrographs of dispersed neat MWNT, A-MWNT(12 h) and A-MWNT(24 h) in DMF. Each sample, contains about same amount of MWNTs. Following blending, the left bottle (neat MWNT) contained black sediment was clearly separated from DMF. The middle and right bottles (A-MWNT for 12 or 24 h) contained homogenous a phase solution after more than a week.

Degree of Miscibility of PU/MWNTs Nanocomposite

FT-IR Analysis. The FT-IR spectra of PU and MWNT nanocomposites were analyzed to elucidate the effects of nanotubes on the formation of hydrogen bonds. Figures 4 (A to D) plot their scale-expanded FT-IR spectra and those of the nanocomposites. Two main regions are of interest in this study, –NH (3200–3500 cm^{-1}) and –C=O (1637–1750 cm^{-1}) stretching. The degree of hydrogen bonding in the PU polymers is determined from their infrared spectra. The functional groups in order of increasing wave numbers, they are H-bonded carbonyl groups in ordered soft domains (1624–1656 cm^{-1}), H-bonded carbonyl groups in ordered hard domains (1699–1706 cm^{-1}), H-bonded carbonyl groups in disordered domains (1710–1718 cm^{-1}), and non-H-bonded (free) carbonyl groups (1730–1733 cm^{-1}), respectively. Figure 4A reveals that the –NH absorption peak at 3300–3263 cm^{-1} is associated with hydrogen-bonded –NH groups between the A-MWNTs and urethane. As A-MWNT content increases, the stretching band shifts to a lower wavenumber that is caused by intermolecular H-bonding in these nanocomposites. Figure 4C displays the infrared spectra of nanocomposite of PU mixed with a constant amount of 10 wt % of A-MWNT within 24 h of acid treatment in the region 2700–3800 cm^{-1}. The –OH group on the MWNTs form hydrogen bonds with the PU. The hard segment has an NH group, and so has stronger hydrogen bonds with A-MWNTs than does the soft segment. The wave number of the absorption peak of the –NH functional group shifted down ware about 42 cm^{-1}, verifying the increase in the numbers of hydrogen bonds. Figure 4B presents the infrared spectra in the region 1650–1800 cm^{-1} for a nanocomposite of PU that contains various A-MWNT(24 h). The neat PU and PU/MWNT nanocomposites show a split broad band centered at 1730 and 1710 cm^{-1}. These peaks arise form non-H-bonded carbonyl groups and the H-bonded carbonyl groups in disordered hard segment domains, respectively. As mentioned above, the extent of the carbonyl group participating in hydrogen bonding is expressed by HBI, which is defined as the relative absorbances of two carbonyl peaks.[22]

$$\mathrm{HBI} = A_{\mathrm{C=O,\ bonded}}/A_{\mathrm{C=O,\ free}} \quad (1)$$

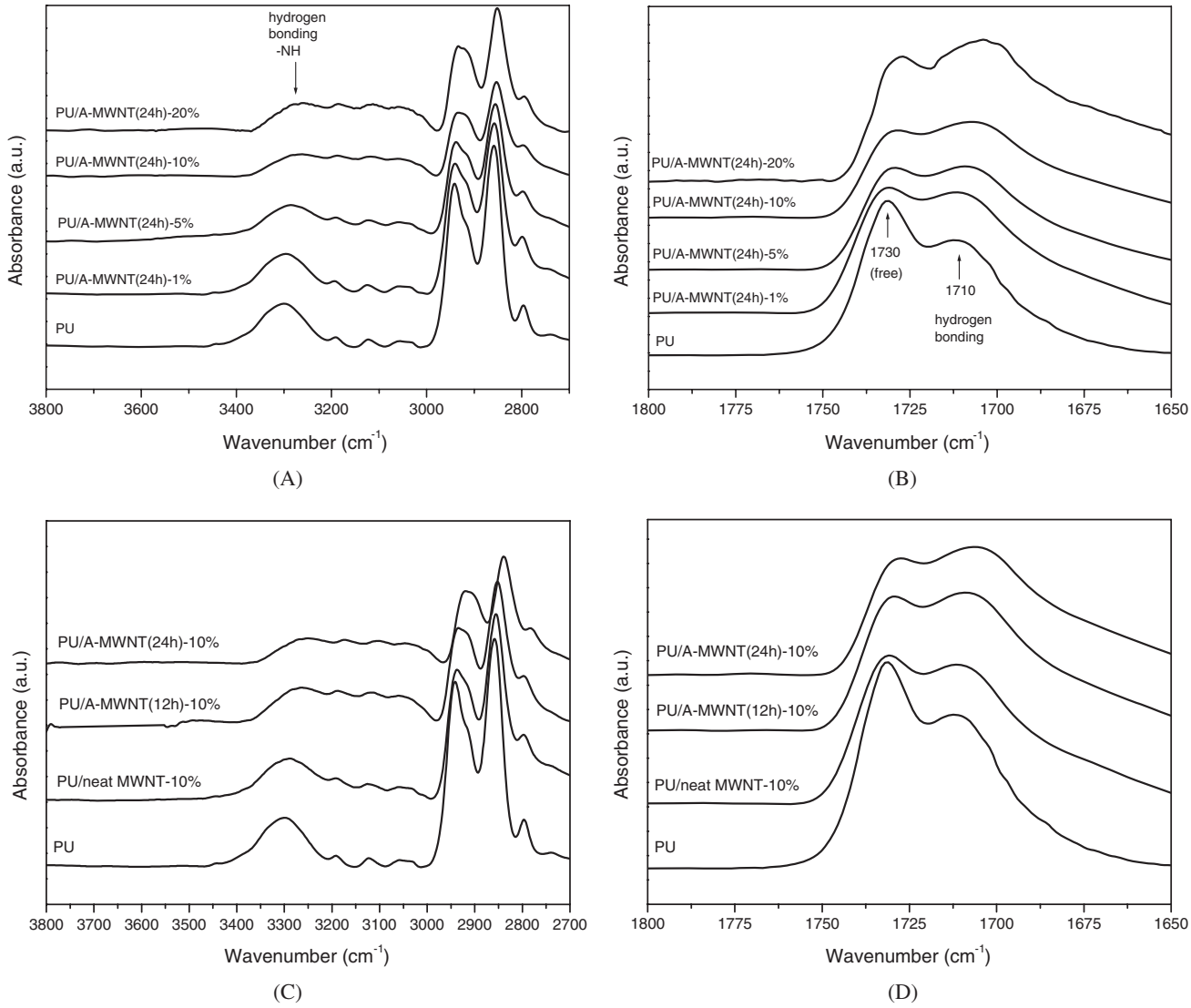

Figure 4. (A) FT-IR spectra of the amino groups of PU/A-MWNT nanocomposites with various A-MWNTs content. (B) FT-IR spectra of the carbonyl groups of PU/A-MWNT nanocomposites with various A-MWNTs content. (C) FT-IR spectra of the amino groups of PU/MWNT nanocomposites with various acid treatment time. (D) FT-IR spectra of the carbonyl groups of PU/MWNT nanocomposites with various acid treatment time.

Where $A_{C=O,\ bonded}$ and $A_{C=O,free}$ are the absorbances of bonded and free carbonyl group, respectivity. All these carbonyl group wavenumbers of nanocomposites, split into two bands at 1730 and 1710 cm^{-1}, corresponding to the free and the hydrogen-bonded carbonyl group, which can be fitted well to the Gaussian function.[26,27] The HBI can be calculated by eq 1 resulting from curve fitting of absorbances of two carbonyl peaks. Table III summarizes the HBI of some PU/MWNT nanocomposites. The HBI of PU/MWNT nanocomposites is found to range from 1.00 for neat polyurethane to 1.88 of PU/MWNT nanocomposites. That result indicateds that the numerical values of HBI (A_{1710}/A_{1730}) were increased with the acid-treatment period and the proportion of A-MWNT percentages in the PU matrix. Those HBI values of the nanocomposites exceed those of plain PU, suggesting that A-MWNTs increased the degree of hydrogen bonding and reduced the phase separation between MWNT and PU. Figure 4C and Figure 4D presents the infrared spectra of nanocomposites of PU/MWNTs that contains 10 wt % A-MWNTs after various periods of

Table III. HBI of PU/MWNT nanocomposites

Designation	HBI = H bonded (1730 cm^{-1}) /H free (1710 cm^{-1})
PU	1.00
PU/neat MWNT-10 wt %	1.14
PU/A-MWNT(12 h)-10 wt %	1.39
PU/A-MWNT(24 h)-1 wt %	1.20
PU/A-MWNT(24 h)-5 wt %	1.37
PU/A-MWNT(24 h)-10 wt %	1.62
PU/A-MWNT(24 h)-20 wt %	1.88

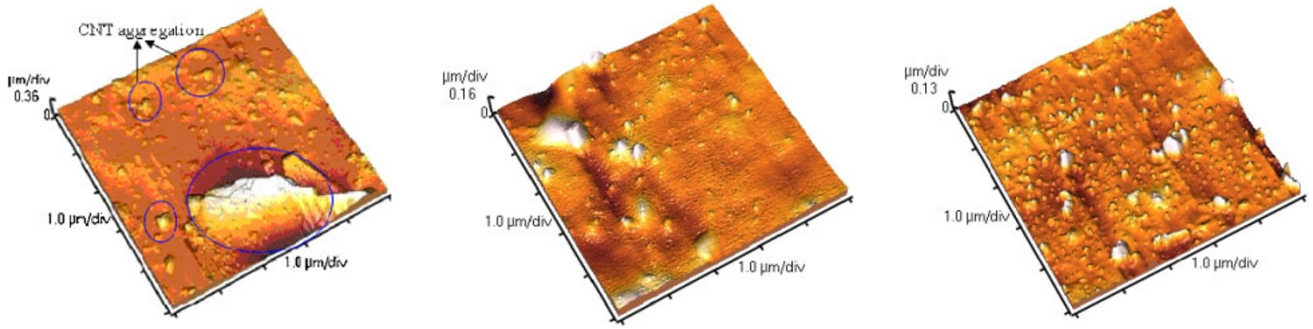

(a) (b) (c)

Figure 5. AFM micrographs of PU/MWNT nanocomposites with 5 wt % A-MWNT with time (a) 0 h, (b) 12 h, (c) 24 h.

acid treatment in the regions 2700–3800 cm^{-1} and 1650–1800 cm^{-1}, respectively. The degree of hydrogen bonding increased with the duration of acid treatment. Since the number of functional groups (–COOH) increased with duration of acid treatment, the number of available sites for hydrogen bonding with PU increased. The high miscibility of PU and A-MWNTs in the nanocomposite was expected to promote the dispersion of A-MWNTs in the PU matrix. The following section will present supportive morphologies of the nanocomposites of PU/A-MWNTs to verify the extensive dispersion of A-MWNTs in the PU matrix.

Morphology. The homogenous dispersion of MWNTs in the PU matrix is one of the most important requirements for strong mechanical reinforcement because inhomogeneites are present as structural defects in the composite material. The former section on miscibility revealed strong interaction between PU and A-MWNTs. In this section, a series of AFM and TEM microphotographs are presented demonstrating the effective dispersion of MWNTs in PU matrix. The AFM images reveal the surface morphology of nanocomposites of PU/MWNT. Figures 5a–c displayed the AFM top view images of the surface of nanocomposite films of PU/MWNTs containing 5 wt % MWNTs, after various periods of acid treatment. Figure 5a shows the PU/neat MWNT sample, indicating a the aggregation of neat MWNT in a PU matrix. Figure 5b shows the AFM image of 5% of A-MWNT(12 h) in a nanocomposite, which demonstrates a slight aggregation of A-MWNT in PU matrix. Figure 5c displays an AFM image of the nanocomposite with 5% of A-MWNT(24 h), revealing that the degree of dispersion of A-MWNT inside the PU matrix exceeds that in both neat MWNT and A-MWNT(12 h). The discussions of the miscibility, established the poor miscibility between PU and neat MWNT. Comparing with the weak interaction of PU and neat MWNT (low hydrogen bonds with PU), indicates that PU/A-MWNTs exhibit a stronger interaction. The TEM micrographs indicated the morphology of the matrix of the nanocomposites of PU/MWNTs. Figure 6a shows a TEM micrograph of PU/neat MWNT, suggesting again the consecutive aggregation of neat MWNT in PU matrix. Figure 6b and c referring to the PU/A-MWNT system, reveal well dispersed A-MWNTs in the PU matrix.

Thermal Properties

Table IV presents the glass transition temperatures of the soft and hard segment (T_{gl}, T_{gh}) of PU and PU/MWNTs nanocomposites with various MWNT compositions measured from MDSC. The glass transition temperatures of nanocomposites increased with MWNTs content, indicting that introducing the glass transition temperature as corresponding to results indicate that the addition of nanotubes significantly improved the thermal properties of nanocomposites in the purging nitrogen.

The T_{gh} of the plain PU is 99.8 °C. In the nanocomposite, the T_{gh} range of the PU/neat MWNTs system is around 100 °C. In the PU/A-MWNTs(12 h) series, T_{gh} was increased with the amount of A-MWNT(12 h). The same results were observed form the PU/A-MWNT(24 h) series. The glass temperatures of the PU/A-MWNT(24 h) system were increased by the interaction (hydrogen bonding) between the PU polymers and the small rod-like molecules, which significantly increased the glass temperature of matrix polymers that were well dispersed inside the matrix. Similarly, reported 2D layered (hydrogen bonding with polymer and clay) silicates (such as clay) can effectively reinforce the polymer matrix,[26] in which the polymer chains are considerably constricted by their confinement within 2D nanoclay platelets, increasing the T_g of the nanocomposites.[27,28] In the system herein, the strong interaction (hydrogen bonding) between the urethane group (–OOCNH–) of PU and the carbonyl acid (–COOH) group in A-MWNTs also constrains the motion of the PU molecules. Therefore, the series of PU/A-MWNTs nanocomposites had

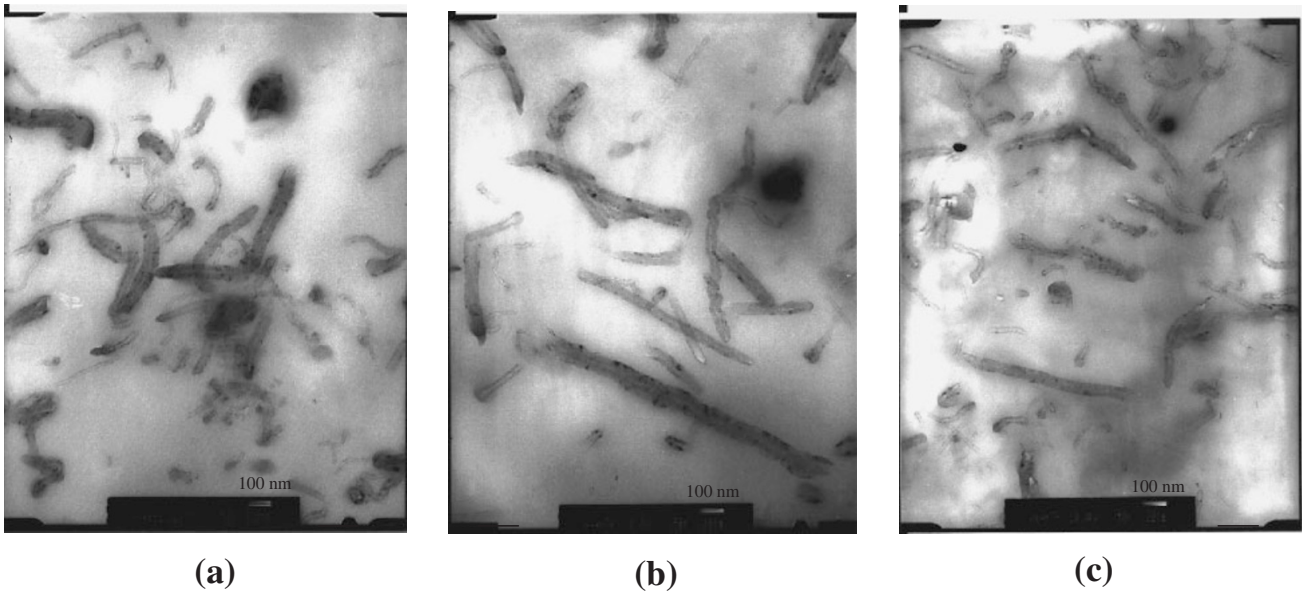

Figure 6. TEM micrographs of PU/A-MWNT nanocomposites with 5 wt % A-MWNT (a) 0 h, (b) 12 h, (c) 24 h.

Table IV. The physical properties of PU/MWNT nanocomposites

Designation	T_{gl}[a] (°C)	T_{gh}[b] (°C)	T_d[c] (°C)	Residue[d] (wt %)	Tensile strength (MPa)	Young's modulus (MPa)	Elongation at break (%)	Electronic conductivity (S/cm)
PU	−45.6	99.8	308.0	6.4	10.3 ± 0.5	9.2 ± 0.3	684.9 ± 5.2	$<10^{-14}$
PU/neat MWNT-1%	−45.7	100.4	311.5	9.8	10.4 ± 0.3	10.3 ± 0.2	514.7 ± 3.5	5.4×10^{-9}
PU/neat MWNT-5%	−44.9	100.7	309.8	13.6	10.2 ± 0.3	15.2 ± 0.3	527.9 ± 5.5	9.0×10^{-7}
PU/neat MWNT-10%	−45.6	100.3	303.4	22.2	11.8 ± 0.7	27.5 ± 0.7	512.0 ± 5.3	5.8×10^{-6}
PU/neat MWNT-20%	−45.3	99.9	302.1	32.6	11.5 ± 0.5	66.2 ± 0.9	237.6 ± 6.7	6.6×10^{-6}
PU/A-MWNT(12 h)-1%	−45.4	105.4	307.7	9.3	10.5 ± 0.3	11.5 ± 0.5	702.4 ± 8.2	4.6×10^{-7}
PU/A-MWNT(12 h)-5%	−44.5	110.7	307.3	11.7	13.6 ± 0.5	15.2 ± 0.3	651.3 ± 7.2	2.3×10^{-5}
PU/A-MWNT(12 h)-10%	−45.3	113.5	306.7	18.3	17.1 ± 0.8	25.5 ± 0.8	583.3 ± 4.8	1.7×10^{-3}
PU/A-MWNT(12 h)-20%	−43.9	118.7	302.1	26.5	18.8 ± 0.7	55.6 ± 0.9	158.9 ± 6.5	7.6×10^{-3}
PU/A-MWNT(24 h)-1%	−43.9	106.6	319.2	7.8	10.8 ± 0.5	12.1 ± 0.9	821.3 ± 9.2	1.7×10^{-6}
PU/A-MWNT(24 h)-5%	−43.7	112.9	315.3	9.4	15.8 ± 0.9	14.8 ± 0.5	709.1 ± 8.5	9.0×10^{-5}
PU/A-MWNT(24 h)-10%	−44.3	120.7	313.1	16.4	17.8 ± 0.8	21.5 ± 1.2	600.1 ± 8.9	3.1×10^{-2}
PU/A-MWNT(24 h)-20%	−44.1	122.5	309.2	23.7	19.7 ± 0.4	51.3 ± 1.5	85.1 ± 3.5	6.2×10^{-2}

[a]Glass temperature of soft domain of Nanocomposite. [b]Glass temperature of hard domain of Nanocomposite. [c]Temperature at 5% weight loss obtained from TGA curve. [d]Residue at 600 °C obtained from TGA curve.

higher T_{gh} than the neat MWNT system. However, the T_{gh} of the nanocomposites of PU/A-MWNTs increased with the duration of acid treatment because the strength of the interaction increased with number of H-bondable sites (acid treatment time) of A-MWNTs. Accordingly, the T_{gh} of PU/A-MWNT(24 h) (120.7 °C) was increased to 20 °C above that of PU/neat MWNT (99.8 °C).

The thermal stability of plain PU and its composites of A-MWNT(12 h) and A-MWNT(24 h) were investigated by thermogravimetric analyzer (TGA). The degradation behavior of the composites is shown in Table IV. The degradation temperatures (T_d), *i.e.*, the temperatures at 5% weight loss of composites, with the exception of the control material were in the same neighborhood of pure PU (Table IV). Note that the degradation temperatures (T_d) is mostly contributed from by the degradation of organic modifier present in the MWNT. It is also found from Table IV that char residues of MWNT/PU nanocomposites were higher than plain PU.

Mechanical Properties

The mechanical properties were measured, and resulting stress-strain profile presented in Figure 7 and summarized in Table IV. The tensile strength, the elongation at breakage and the Young's modulus of the neat PU matrix were 10.3 MPa, 684.9%, and

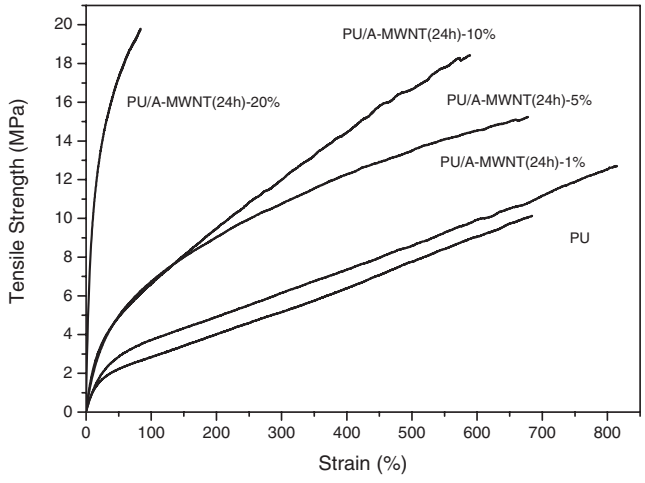

(A)

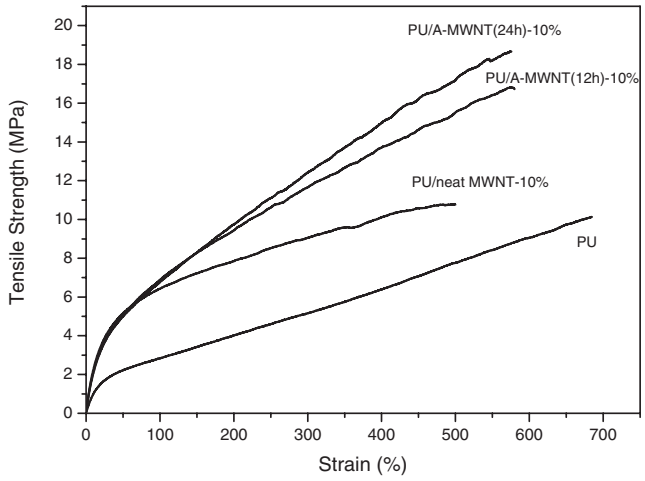

(B)

Figure 7. (A) Stress-strain curves of PU/MWNT nanocomposites with various MWNTs content. (B) Stress-strain curves of PU/MWNT nanocomposites with various acid-treatment period.

9.0 MPa, respectively. The Young's modulus and tensile strength increased up to 466% and up to 91%, respectively, with the blended A-MWNT(24 h). However, the elongation at break of these composites largely decreased with increasing MWNT (see Table IV). The elongations of nanocomposites were considerably altered. The reason for the sharp drop in elongation in the nanocomposites is not clear but might come from the appearance of the stress concentration regions introduced by the nanotube bundles or larger agglomerates at higher weight loadings. In particular, composites containing MWNTs and A-MWNT(12 h) resulted in a greater increased Young's modulus compared with A-MWNT(24 h), indicating that severe surface modification etching lowers mechanical properties (Young's modulus). These increases in the mechanical properties might be due to the reinforcing effect of MWNT and A-MWNT in the PU matrix. However, these mechanical properties of the PU/A-

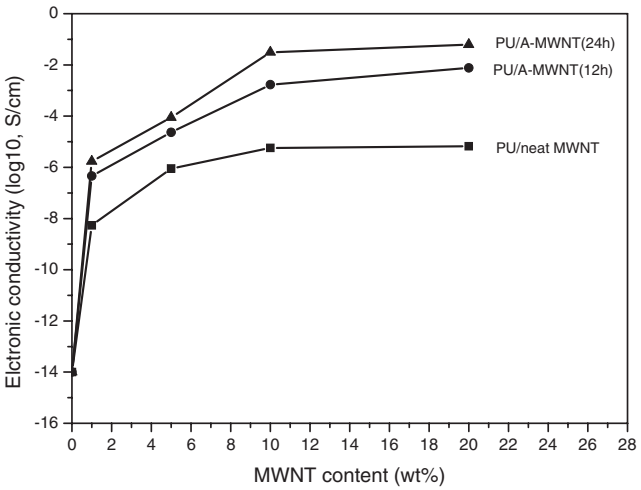

Figure 8. Electronic conductivity of PU/MWNT nanocomposites.

MWNT composites were also superior to those of the PU/MWNT composites. The higher mechanical properties of PU/A-MWNT can perhaps be attributed to the higher content of –COOH groups of A-MWNT inducing the higher interfacial interactions between A-MWNT and PU molecular chains. The tensile strength and the Young's modulus of nanocomposite increased with A-MWNT(24 h) content. The interaction between the functional group (–COOH) of A-MWNT(24 h) and the urethane group (–OOC–NH–) of PU enhance the capability of A-MWNTs to reinforce a PU matrix. The mechanical properties of nanocomposite improved as the percentages of A-MWNT(24 h) increased. Consequently, Figure 7B plots the stress-strain curves of PU blended with various time of acid treatment of MWNTs amount 10 wt %, showing better tensile strength and Young's modulus improved as the period of acid treatment of the MWNTs increased.

Electronic Conductivity

Figure 8 shows the electronic conductivity of the nanocomposite based on PU for various percentages of MWNT. The electronic conductivity of plain PU is 10^{-14} S/cm. The electronic conductivity of the nanocomposite of PU/neat MWNT increased with the neat MWNT content (from 10^{-14} to 6.6×10^{-6} S/cm). The conductivity of the nanocomposite based on PU and A-MWNTs increases more efficiently (from 10^{-14} to 0.062 S/cm). The nanocomposites prepared from blending of acid-treated MWNTs with PU exhibited greater electronic conductivity than that obtained by mixing the same amount of neat MWNT with PU, because A-MWNTs disperse more effectively in a PU matrix than that do neat MWNT. A conductive polymer based on PU can thus be obtained by blending with the acid-treated MWNT.

CONCLUSIONS

MWNTs-reinforced PU nanocomposites with excellent mechanical properties, thermal properties and electric conductivity have been successfully prepared by simple solution blending. This study showed that hydrogen bonding played an important role on the mechanical properties and that MWNTs had a strong influence on hard segment hydrogen bonding. We used the concentrated acids to treat the multi-walled carbon nanotubes to create functional groups (–COOH) on the surface of MWNTs. A high miscibility through the formation hydrogen bondings between PU and MWNTs of nanocomposite can be characterized from FT-IR spectra. The morphology tells that there is a well dispersed A-MWNTs presented in PU matrix. A high T_g nanocomposite (120.7 °C) compared to neat PU (99.8 °C) was prepared from the thermal characterization. The tensile strength and Young's modulus of nanocomposites (PU/A-MWNT(24 h)-20 wt %) increase 91% and 466%, respectively. The nanocomposites with 1.5 wt % A-MWNT present led to 12–13 orders increase in the electrical conductivities. We obtained nanocomposites with superior thermal and mechanical properties compared with plain PU due to the homogenous dispersion of A-MWNTs in PU matrix.

Acknowledgment. The authors acknowledge with gratitude financial support from the National Science Council, Taiwan R. O. C. through grant No. NSC92-2216-E-224-003. We also thank Prof. K. S. Ho for providing MWNTs material and for many helpful discussions.

REFERENCES

1. S. Iijima, *Nature*, **56**, 354 (1991).
2. F. Tsui, L. Jin, and O. Zhou, *Appl. Phys. Lett.*, **76**, 1452 (2000).
3. M. F. Lin, F. L. Shu, and R. B. Chen, *Phys. Rev. B: Condens. Matter Mater. Phys.*, **61**, 14114 (2000).
4. Z. W. Pan, S. S. Xie, and L. Lu, *Appl. Phys. Lett.*, **74**, 3152 (1999).
5. J. Chen, M. A. Hamon, H. Hu, Y. Chen, A. M. Rao, P. C. Eklund, and R. C. Haddon, *Science*, **282**, 95 (1998).
6. S. Niyogi, M. A. Hamon, H. Hu, B. Zhao, P. Bhowmik, R. Sen, M. E. Itkis, and R. C. Haddon, *Acc. Chem. Res.*, **35**, 1105 (2002).
7. Y. Lin, A. M. Rao, B. Sadanadan, K. E. A. Ken, and Y. Sun, *J. Phys. Chem. B*, **106**, 1294 (2002).
8. S. L. Ruan, P. Gao, X. G. Yang, and T. X. Yu, *Polymer*, **44**, 5643 (2003).
9. A. B. Dalton, S. Collins, E. Munoz, J. M. Razal, V. H. Ebron, and J. P. Ferraris, *Nature*, **423**, 703 (2003).
10. S. A. Gordeyev, F. J. Macedo, J. A. Ferreira, F. W. J. Hattum, and C. C. Bernardo, *Phys. B*, **279**, 33 (2000).
11. Z. Jin, K. P. Pramoda, G. Xu, and S. H. Goh, *Chem. Phys. Lett.*, **337**, 43 (2001).
12. M. L. Chapelle, C. Stephan, T. P. Nguyen, S. Lefrant, C. Journet, P. Bernier, E. Munoz, A. Benito, W. K. Maser, M. T. Martiner, G. F. Fuente, T. Guillard, G. Flaant, L. Alvarez, and D. Laplaze, *Synth. Met.*, **103**, 2510 (1999).
13. Z. Jia, Z. Wang, C. Xu, J. Liang, B. Wei, D. Wu, and S. Zhu, *Mater. Sci. Eng., A*, **103**, 2510 (1999).
14. L. S. Schadler, S. C. Ciannaris, and P. M. Ajayan, *Appl. Phys. Lett.*, **73**, 3842 (1998).
15. F. H. Gojny, J. Nastalczyk, Z. Roslaniec, and K. Schulte, *Chem. Phys. Lett.*, **370**, 820 (2003).
16. X. J. Xu, M. M. Thwe, C. Shearwood, and K. Liao, *Appl. Phys. Lett.*, **81**, 2833 (2002).
17. D. Quan, E. C. Dickey, R. Andrews, and T. Rantell, *Appl. Phys. Lett.*, **76**, 2868 (2000).
18. B. K. Zhu, S. H. Xie, Z. K. Xu, and Y. Y. Xu, *Compos. Sci. Technol.*, **66**, 548 (2006).
19. W. D. Zhang, L. Shen, I. Y. Phang, and T. Liu, *Macromolecules*, **37**, 256 (2004).
20. J. Kwon and H. D. Kim, *J. Polym. Sci., Part A: Polym. Chem.*, **43**, 3973 (2005).
21. H. C. Kuan, C. C. M. Ma, W. P. Chang, S. M. Yuen, H. H. Wu, and T. M. Lee, *Compos. Sci. Technol.*, **65**, 1703 (2005).
22. R. W. Seymour, G. M. Estes, and S. L. Cooper, *Macromolecules*, **6**, 48 (1973).
23. M. M. Coleman, D. J. Skrovanek, J. Hu, and P. C. Painter, *Macromolecules*, **21**, 59 (1988).
24. S. L. Huang and J. Y. Lar, *Eur. Polym. J.*, **33**, 1563 (1997).
25. N. I. Kovtyukhova, T. E. Mallouk, L. Pan, and E. C. Dickey, *J. Am. Chem. Soc.*, **125**, 9761 (2003).
26. Y. Kojima, A. Usuki, M. Kawasumi, A. Okada, Y. Fukushima, T. Kurauchi, and O. Kamigaito, *J. Mater. Res.*, **8**, 1185 (1993).
27. R. Krishnamoorti, R. A. Vaia, and E. P. Giannelis, *Chem. Mater.*, **8**, 1728 (1996).
28. H. B. Lu and S. Nutt, *Macromol. Chem. Phys.*, **204**, 1832 (2003).